DOI: 10.21062/mft.2023.075 http://www.journalmt.com

The Mechanical Analyses and Structural Optimization of CSMC Preload System under Multi-Load Cases

Xianewei Wang (0000-0001-9804-0403)[1], Haikuo Zhao (0009-0000-8454-2656)[1], Fei Xie (0000-0002-5484-3228)[2], Chenyang Li (0009-0008-7418-6115)[1], Xiulian Li (0000-0001-9441-261X)[1]
[1]Jiangsu University of Technology, Changzhou 213001, China. E-mail: wangxw@jsut.edu.cn, 1262734188@qq.com, 936303415@qq.com, haikuo1412@163.com
[2]Shunde Polytechnic, Foshan 528000, China. E-mail: jeffrey_xie@163.com

In order to accumulate experience in the design and manufacturing of the toroidal field coils for the China Fusion Engineering Test Reactor, a model coil of mixed Nb_3Sn-NbTi superconducting magnet with a maximum magnetic field variation rate of 1.5 T/s has been developed at the Institute of Plasma Physics, Chinese Academy of Sciences. The preload system, as one of the key components of the model coil, plays a crucial role in maintaining the overall integrity and stability of the model coil. First the magnetic field and electromagnetic forces of the model coil under extreme conditions are calculated based on Maxwell's equations. Then, the mechanical performance of the model coil at room and cryogenic temperatures is analyzed. To addressing the issue of excessive stress in the preload components of the model coil under preload, several optimization design schemes are proposed and iteratively analyzed. Finally, stress linearization is performed, and stress evaluation is conducted based on the analytical design. The assessment results indicate that certain optimization schemes enable the preload components to fully meet the operational requirements at both room and cryogenic temperatures. The outcomes presented in the paper will provide reference for the subsequent design and manufacturing of the central solenoid coil.

Keywords: CSMC, Preload components, Winding pack, Stress linearization, Structural optimization

1 Introduction

The China Fusion Engineering Test Reactor (CFETR) is a new tokamak device with engineering & physics parameters falling between ITER and DEMO. To accumulate experience in developing the central solenoid coil for CFETR, the Institute of Plasma Physics Chinese Academy of Sciences created a model coil, known as the Nb_3Sn-NbTi hybrid superconducting magnet model coil (CSMC), with a maximum magnetic field of 12 Tesla and a maximum magnetic field ramp rate of 1.5 Tesla per second. The research of CSMC focused on three aspects: 1) exploration of superconducting magnet winding and insulation manufacturing processes; 2) study of superconducting joint performance; 3) investigation of superconducting and quenching properties of the conductor. The CSMC are comprised mainly by winding packs, insulation system, cooling system, current leads, buffer zone and preload system, as shown in Figure 1. Given the excellent electromagnetic and mechanical properties of Nb_3Sn and NbTi superconducting cables [1-3], as well as the favorable self-supporting performance of Cable-In-Conduit Conductors (CICCs) [4-6], the high-field region of CSMC employs Nb_3Sn conductor, while the low-field region employs NbTi conductor. The high-field coil includes both inner and outer Nb_3Sn coils, while the low-field coil consists of upper, middle, and bottom NbTi coils. The cryogenic system utilizes liquid nitrogen and helium coolants to provide a low temperature operating environment for CSMC. The current leads, comprising of single and double leads, act the function of transmitting the current. Buffer components are installed on the upper and lower surfaces of the winding modules to maintain the axial alignment of Nb_3Sn and NbTi coils. These components could avoid damage to the winding modules induced by the axial compression loads. The preload system is comprised by load beams, compression plates, and tension rods. The tension rods include the inner and outer rods arranged in the toroidal direction. The preload is applied through super bolts on the two ends of tension rod. The load beam connects the inner and outer tension rods and converts the tensile stress of the bolt into compressive stress on the winding modules. To evenly distribute the preload onto the winding modules, a compression plate with a thickness of 100 mm is amounted below the load beam. The compression plate is radially and circumferentially segmented to prevent significant eddy current losses induced by time-varying magnetic fields. These segmented sector-shaped compression plates are isolated from each other, thereby confining eddy currents to a small region.

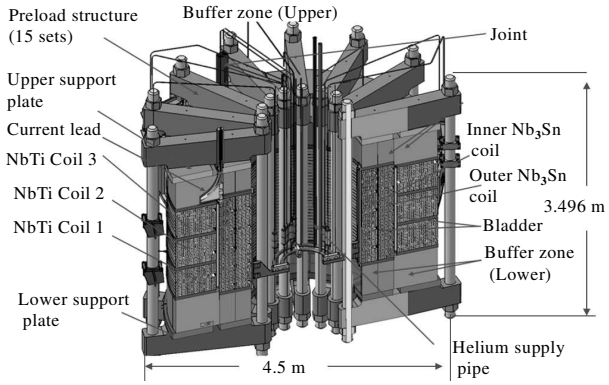

Fig. 1 *The geometric structure of CSMC*

2 The load description

The load on the CSMC can be categorized based on its operational phases: i) Room Temperature Phase: During this phase, the CSMC primarily bears the preload. The applying of preload reference International Thermonuclear Experimental Reactor (ITER) CSMC and Central Solenoid (CS) [7-9]. To ensure the overall integrity of the CSMC after energization and to prevent insulation components from tearing down, a total preload of 75 MN is applied at room temperature. This preload is evenly distributed across 15 sets of tension rods, namely each tension rod carries a preload of 2.5 MN. ii) Cooling Phase: The CSMC is cooled from room temperature to an ultra-low temperature of 4.5 K in two steps. The entire cooling process spends over 21 days. First, liquid nitrogen is employed to bring the CSMC's temperature down to 80 K from room temperature, followed by a transition to 4.5 K using supercritical helium forced-flow cooling. This gradual cooling process could effectively prevent significant thermal gradients between the coils. However, due to differences in thermal contraction coefficients among the components of CSMC, there will inevitably be thermal stresses caused by the inconsistent thermal shrinkage during the cooling process. The discrepancies in thermal contraction coefficients are the primary reasons for thermal stresses during the cooling phase. iii) Energization Phase: Once the cooling process is completed, the CSMC will be energized. During the steady-state operation, the maximum current through the coil is 47.65 kA. The interaction between the magnetic fields and currents generates substantial electromagnetic forces on the winding modules. These forces lead to radial expansion of the coil while also compressing the winding modules symmetrically around the mid-plane.

3 The electromagnetic analysis of CSMC under the steady state

Once CSMC is energized, a magnetic field will be generated around the coil, and the interaction between the magnetic field and the current will induce electromagnetic forces. For CSMC operating in steady-state conditions, its current reaches the peak of 47.65 kA, corresponding to the maximum magnetic field and electromagnetic forces. The calculation of the magnetic field and electromagnetic forces is based on Ampère's law and Biot-Savart law, respectively. Since the model coil has a hollow cylindrical structure and exhibits symmetry along the toroidal direction, there is only need to create a two-dimensional analysis model to calculate the magnetic field of any cross-sectional plane of CSMC. The solved magnetic field distribution is illustrated in Figure 2, with the maximum magnetic field located on the inner side of the inner Nb_3Sn coil, near the mid-plane, reaching approximately 12 T. The calculation of electromagnetic forces is carried out using the commercial software Maxwell. In order to incorporate the electromagnetic forces into the subsequent mechanical analysis models, a three-dimensional analysis model is created. When setting the boundary conditions for the finite element analysis, master-slave boundary conditions are applied on the left and right sides of the air region, while default boundary conditions are used on the remaining surfaces. The solved electromagnetic force density distribution on the toroidal cross-section of the coil winding is depicted in Figure 3. Corresponding to the distribution of the magnetic field, the maximum electromagnetic force density is also situated near the mid-plane on the inner side of the inner Nb_3Sn coil. Furthermore, it is evident that the electromagnetic forces cause radial expansion of the coil windings and axial compression with the mid-plane as the symmetry plane.

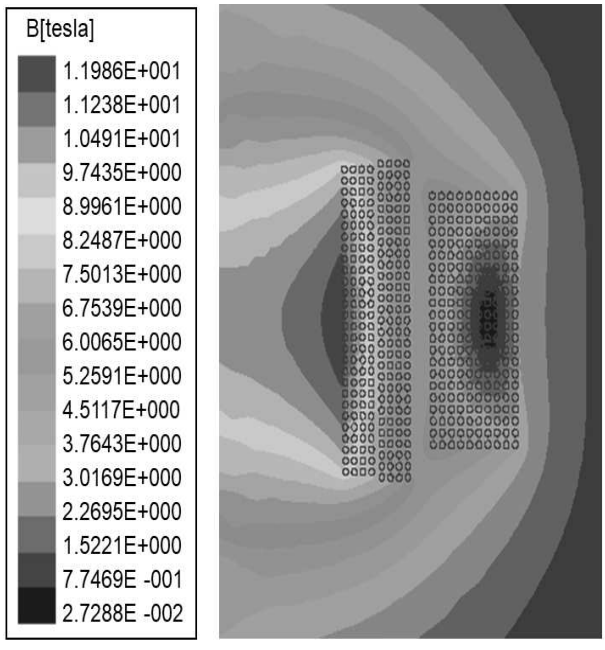

Fig. 2 *The magnetic density of the winding packs*

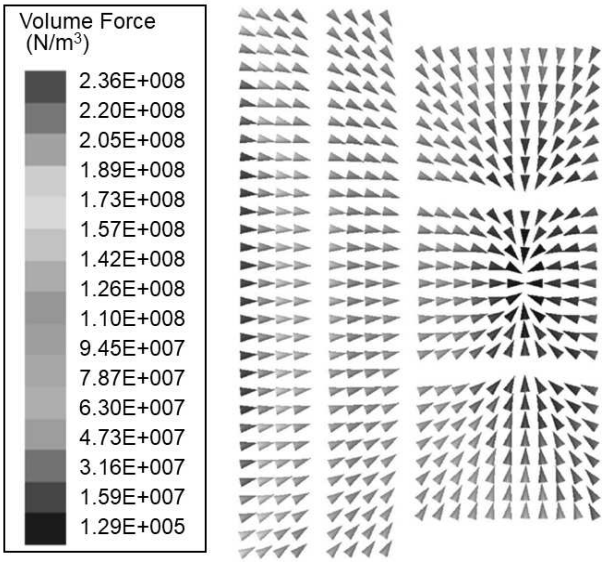

Fig. 3 *The electromagnetic force density of the winding packs*

4 The mechanical analysis of the preload components under multi-load cases

Due to the structural symmetry of CSMC in the toroidal direction, enhancement of computational efficiency in the mechanical analysis can be achieved by simplifying the analysis model, namely creating a 1/15 coil, as shown in Figure 4. Additionally, since the mechanical analysis primarily focuses on CSMC's preload system, there is no need to create the detailed CICC model for the winding packs. Instead, equivalent material properties are utilized, and the properties are calculated based on the homogenization theory [10-11]. And the material properties of CSMC at 4.5 K are listed in Table 1. As CSMC is anchored through base bolts, fixed constraints are applied to the bottom of the load beams in the finite element analysis [12-13]. The coil experiences various loads, including preload, thermal, and electromagnetic loads. The preload is applied through the super bolts at both ends of the tension rods. In the finite element analysis, the preload is simulated by employing preload elements. During the cooling process, the thermal loads caused by temperature gradients is disregard due to the slow cooling process. However, because of the differing thermal contraction coefficients between CSMC's preload components and the insulation components, thermal loads will unavoidably emerge during the cooling process. The applying of thermal loads is achieved by defining reference temperature and material thermal contraction coefficients.

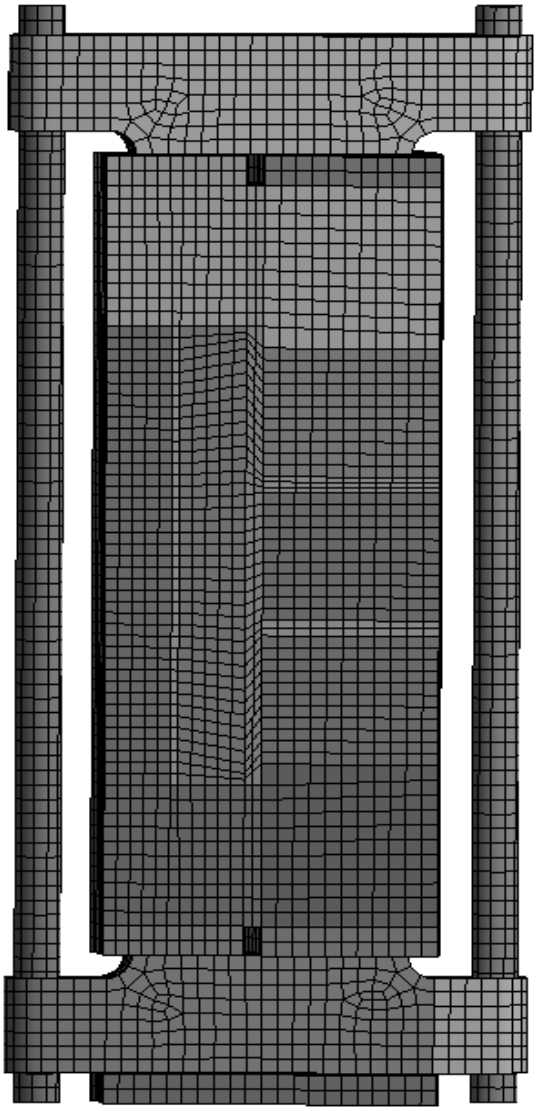

Fig. 4 *The 1/15 finite element model of CSMC*

Tab. 1 *Material properties at 4.5 K*

Properties	316LN SS	Insulation	Nb_3Sn WP	NbTi WP
E_x (GPa)	207	12	48.2	48
E_y (GPa)		20	48.2	48
E_z (GPa)		20	121.7	119.5
G_{xy} (GPa)	79.6	6	7.22	6.9
G_{xz} (GPa)		6	16.1	16.5
G_{yz} (GPa)		6	20.9	20.3
PR_{xy}	0.3	0.33	0.30	0.30
PR_{yz}		0.17	0.12	0.12
PR_{xz}		0.33	0.12	0.12
CTE_x (%)	0.29	0.70	0.31	0.31
CTE_y (%)		0.25	0.31	0.31
CTE_z (%)		0.25	0.29	0.30

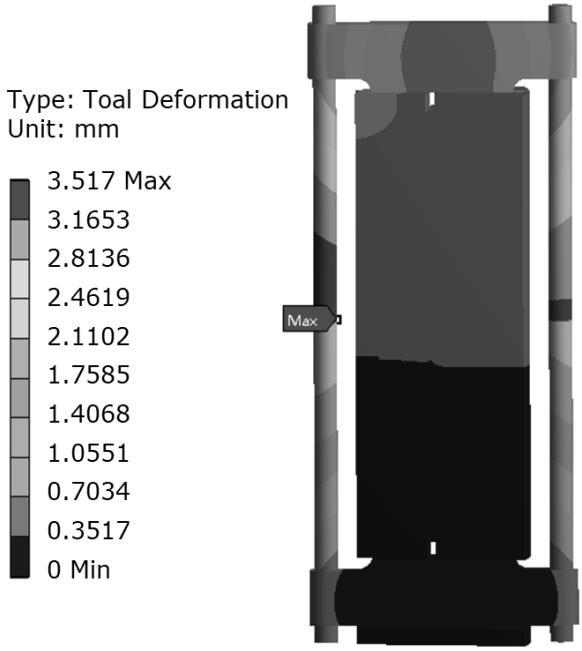

Fig. 5 *The room temperature deformation of CSMC under preload*

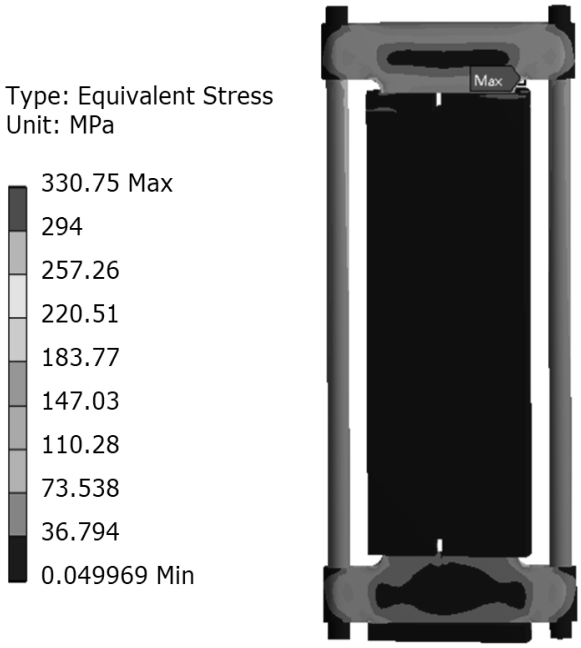

Fig. 6 *The equivalent stress of CSMC under preload*

After energization, the interaction between the magnetic field and electromagnetic forces will generates varying electromagnetic loads. The electromagnetic force density computed in Maxwell can be directly input into the finite element model. Conservatively, the mechanical analysis for the preload components is performed under the extreme electromagnetic force. It's worth noting that the mechanical properties of stainless steel 316 LN, such as tensile strength and yield strength, are higher at low temperatures than that of room temperature. Therefore, the preload components are more susceptible to failure at room temperature. Figures 5, 6, and 7 show the stress and deformation of CSMC at room temperature and 4.5 K. It is indicated that under the influence of preload, the preload components do not undergo significant deformation. The maximum stress occurs on the upper load beam, with a peak value of 331 MPa. Under the combined influence of preload, thermal, and electromagnetic loads at 4.5 K, the maximum equivalent stress appears on the lower load beam, reaching the peak value of 361 MPa.

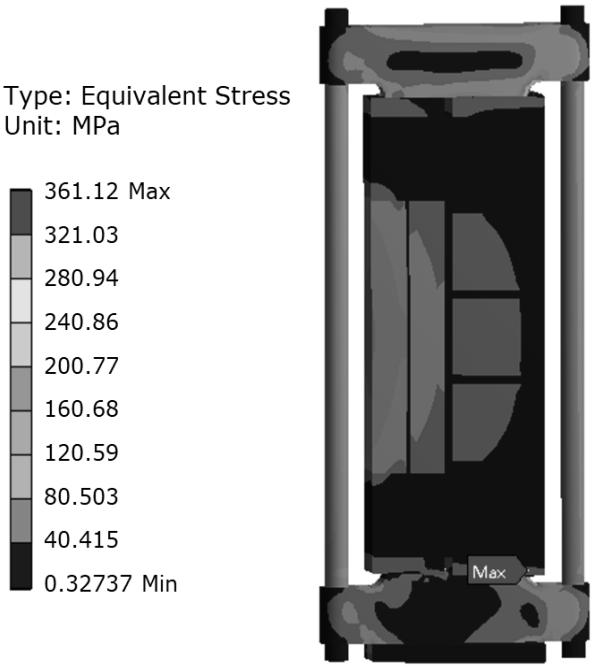

Fig. 7 *The equivalent stress of CSMC under P+T+E*

5 The structural optimization of the preload system

Due to the excessive equivalent stress on the load beam under the preload, it is necessary to optimize the preload components. Two strategies are proposed. The first strategy involves optimizing the structure and dimensions of the tension rods, as shown in Figure 8. In option (b), the diameter of the middle region of the tension rod is increased to 160 mm, with smooth transitions between the mid-section and the ends of the rod. In option (c), the diameter of the middle region of the tension rod is also increased to 160 mm, but with a vertical transition at the mid-section and the two ends. Option (d) increases the diameter of the entire tension rod from 140 mm to 160 mm. The second strategy entails optimizing the structure and dimensions of the load beam, as illustrated in Figure 9. In option (b), the ends of the load beam are left not chamfered, maintaining a constant height of 400 mm along its length. In option (c), the ends of the load beam are designed with a combination of straight and convex outer curves.

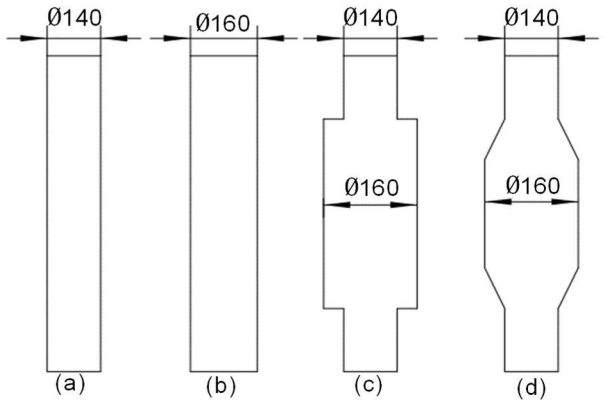

Fig. 8 *The optimization of tension rod*

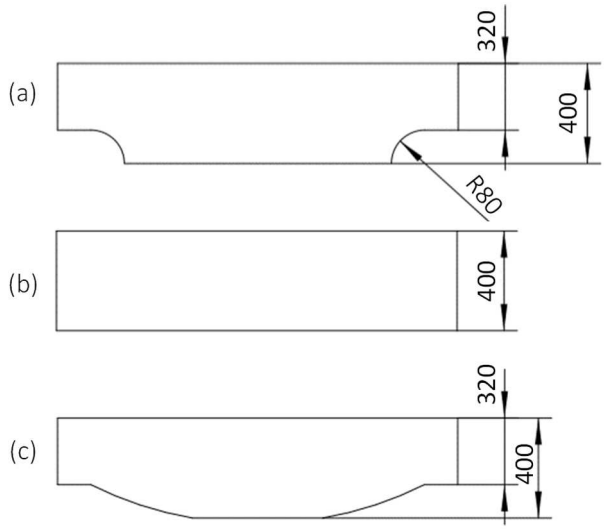

Fig. 9 *The optimization of load beam*

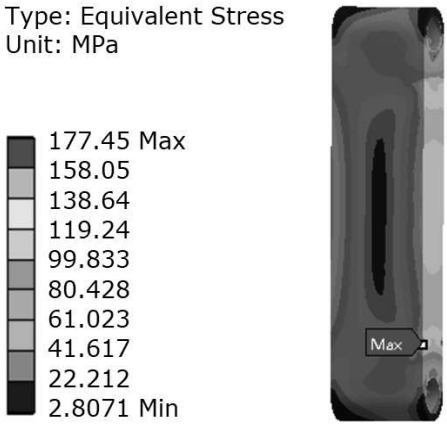

Fig. 10 *The equivalent stress on the load beam with the height of 400 mm*

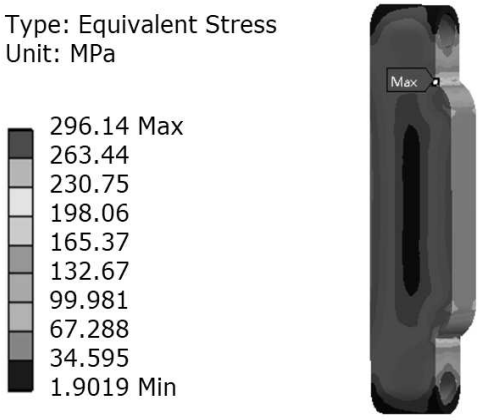

Fig. 11 *The equivalent stress on the optimized load beam*

Tab. 2 *The maximum stress under different schemes*

Equivalent Stress	**Optimization Schemes**						**Threshold**
	(a)-(a)	(a)-(b)	(a)-(c)	(a)-(d)	(b)-(a)	(c)-(a)	
RT-Stress (MPa)	331	329	338	326	211	297	300
4.5 K-Stress (MPa)	361	352	352	361	233	298	1200

When using the n scheme of (a)-(b) for the load beam and tension rod, CSMC experiences a maximum equivalent stress of 329 MPa under room temperature and 352 MPa at 4.5 K. For the scheme of (a)-(c), the maximum equivalent stress is 338 MPa at room temperature and 352 MPa at 4.5 K. Finally, for the scheme of (a)-(d), the maximum equivalent stresses under room temperature and 4.5 K are 326 MPa and 360 MPa respectively. For other schemes, the maximum stresses at room temperature and 4.5 K are listed in Table 2. It is evident that when utilizing the schemes of (b)-(a) and (c)-(a), a significant reduction in maximum stress is observed both at room temperature and 4.5 K shown in Figures 10 and 11.

6 The stress evaluation

The assessment of the stress is based on the analytical design, where stress is categorized into different types such as membrane stress, bending stress, peak stress, and secondary stress. According to the nature of external loads, each type of stress has distinct allowable thresholds, of which the membrane stress must not exceed the design stress strength, And the sum of membrane stress plus bending stress must not exceed 1.5 times the design stress strength. Secondary stress must not exceed 2 times the design stress strength, where the design stress strength is the minimum value between half of the material's tensile

strength and 2/3 of its yield strength.

Referring to the ITER Design Handbook [14-15], the tensile strength and yield strength of stainless steel 316 LN at room temperature are 600 MPa and 300 MPa respectively, while at 4.5 K, they are 1500 MPa and 900 MPa, respectively. Therefore, the design stress strength of 316 LN at room temperature and 4.5 K is 200 MPa and 600 MPa, respectively.

In the finite element analysis software Workbench, stress linearization is used to categorize the equivalent stress into different types for stress assessment. For 316 LN, due to its significantly better mechanical performance at 4.5 K compared to that at room temperature, the stress linearization is performed at room temperature. Figures 12 and 13 present the stress linearization along the thickness direction of the load beam for schemes (b)-(a) and (c)-(a). It is indicated that the overall membrane stress of the load beam in scheme (b)-(a) is about 60 MPa, with a maximum bending stress of approximately 80 MPa. In scheme (c)-(a), the overall membrane stress is around 75 MPa, with a maximum bending stress of about 160 MPa.

According to the limits on different types of stress in the analytical design, the membrane stress for both schemes is less than the design stress strength, and the sum of membrane stress plus bending stress is less than 1.5 times the design stress strength. Table 2 lists the maximum equivalent stresses and stress thresholds of CSMC under six different design schemes. At the temperature of 4.5 K, due to the significant enhancement of the tensile and yield strength of 316 LN, the stress threshold is 1200 MPa. Clearly, all six schemes meet the strength requirements at 4.5 K. However, at room temperature, the maximum stress of four schemes exceeds the stress threshold. Although the maximum stress in scheme (c)-(a) is below the stress threshold, it lacks sufficient safety margin. On the other hand, scheme (b)-(a) not only has a maximum stress below the stress threshold but also has sufficient safety margin. However, it would increase the manufacturing cost of preload components.

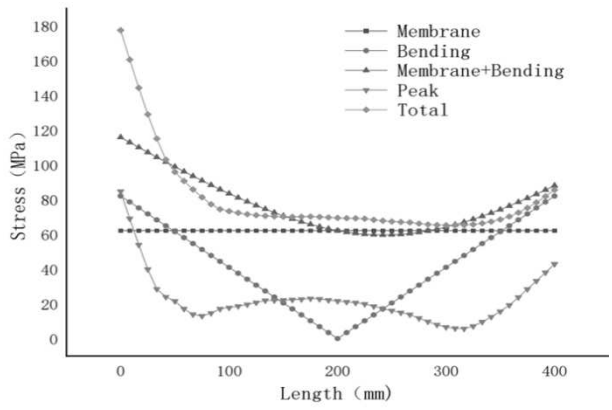

Fig. 12 *The stress linearization of the 400 mm-thick load beam*

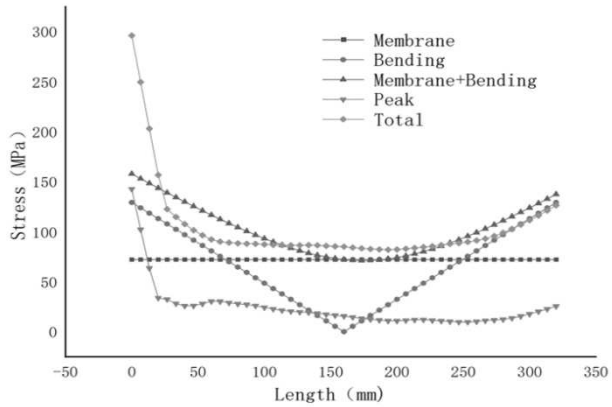

Fig. 13 *The stress linearization of the optimized load beam*

7 Conclusion

When the excitation current of CSMC reaches 47.65 kA, the coil's magnetic field reaches the maximum value of 12 T. The maximum magnetic field occurs within the inner Nb_3Sn coil near the mid-plane. Corresponding to the magnetic field, the maximum electromagnetic force density is about 2.36×108 N/m^3. And it also occurs near the mid-plane of the inner Nb_3Sn coil. In studying the stress state of the preload components under various load conditions, using equivalent material properties for the winding packs can simplify the computational model and improve analysis efficiency. When different design schemes are applied to the load beam and tension rod, categorizing the equivalent stress using stress linearization and conducting stress assessment based on analytical design reveals that all the six schemes meet strength requirements at 4.5 K with sufficient safety margins. At room temperature and under the effect of preload, the equivalent stress of four schemes exceeds the stress threshold. However, increasing the thickness of the load beam at both ends to 400 mm or designing the middle area of the load beam's lower surface as a combination of concave and flat surfaces effectively reduces the maximum stress of the preload components. Among these schemes, increasing the thickness of the load beam has the most noticeable effect on improving the strength of the preload system.

Acknowledgement

This project has been financially supported by the Talent Project of Jiangsu Institute of Technology (Grant No. KYY16002) and the Project of Background Field Magnets (Grant No. KYH20148).

References

[1] HUAWEI JIANG, SONGTAO WU. (2018). Calculation model of coupling loss time constant for Nb_3Sn conductor under cyclic

electromagnetic load. In: *Rare Metal Materials and Engineering*, Vol. 47, No. 10, pp. 2970-2975. Chinese Non-ferrous metal society. China.

[2] QINGHANG QIU, HONGLI SUO, JUNSHENG CHENG, et al. (2020). Fabrication and Superconducting Properties of Nb_3Sn Superconducting Bulks. In: *Chinese Journal of Rare Metals*, Vol. 44, No. 2, pp. 166-171. Chinese Non-ferrous metal society. China.

[3] WEI LUO, FEI LI, MEI WANG, DONGFANG TIAN. (2018). The Statistic Tensile Strength and Failure Probability of Nb_3Sn Strands Considering the Characteristics of Filament Fragmentation. In: *Chinese Journal of Solid Mechanics*, Vol. 39, No. 2, pp. 182-188. The Chinese society of Theoretical and Applied Mechanics. China.

[4] DONGHUA YUE, XINGYI ZHANG,YOUHE ZHOU. (2018). Theoretical analysis for the mechanical behavior caused by an electromagnetic cycle in ITER Nb3Sn cable-in-conduit. In: *Acta Mechanica Sinica*, Vol. 34, No. 4, pp. 614-622. Chinese Academy of Sciences. China.

[5] UGLIETTI D., SEDLAK K., et al. (2018). Progressing in cable-in-conduit for fusion magnets: from ITER to low cost, high performance DEMO. In: *Superconductor Science & Technology*, Vol. 31, No. 5, Art. No.: 055004. IOP. England.

[6] TAKAHATA KAZUYA, MORIUCHI SADATOMO, et al. (2018). Lessons learned from twenty-year operation of the Large Helical Device poloidal coils made from cable-in-conduit conductors. In: *Cryogenics*, Vol. 91, pp. 1-6. Elsevier. Netherlands.

[7] Y. FU, C. JONG, P. MICHAEL, AND N. MITCHELL. (2006). Pre-Compression Requirements for the ITER Central Solenoid. In: *IEEE Transactions on Applied Superconductivity*, Vol. 16, No. 2, pp. 791-794. IEEE. USA.

[8] R BONIFETTO, A BRIGHENTI, T ISONO, et al. (2017). Analysis of the cooldown of the ITER central solenoid model coil and insert coil. In: *Superconductor Science & Technology*, Vol. 30, No. 1, Art. No.: 015015. IOP. England.

[9] TSUJI H, EGOROV S, MINERVINI J, et al. (2001). ITER R&D: Magnets: Central solenoid model coil. In: *Fusion engineering and design*, Vol. 55, No. 2, pp. 153-170. ELSEVIER. Netherlands.

[10] AIHUA XU, YU WU, DAPENG YIN, et al. (2018). Structural Stress Analysis of the CFETR Central Solenoid Model Coil. In: *IEEE Transactions on Plasma Science*, Vol. 46, No. 5, pp. 1512-1516. IEEE. USA.

[11] WU F, LIU XG, GAO X, et al. (2023). An approach of calculating winding pack smeared properties for TF magnets using artificial neural network. In: F*usion engineering and design*, Vol. 192, Art. No.: 113790. ELSEVIER. Netherlands.

[12] XIANEWEI WANG, PENG HAN, QING HE, et al (2019). Induction Brazing Analysis of EAST Fast Control Coil Conductor. In: *Manufacturing Technology*, Vol. 19, No. 5, pp. 896-902. Engineering Village. USA.

[13] XIANEWEI WANG, PENG HAN, QING HE, et al. (2020). The Thermal and Structural Analysis of Vertical Stability Coil. In: *Manufacturing Technology*, Vol. 20, No. 1, pp. 120-125. Engineering Village. USA.

[14] ITER, System Design Description DDD11-12 ITER_D_2MVZNX v2.2, 2009. https://user.iter.org/?uid = 2MVZNX.

[15] ITER, Magnet Structural Design Criteria Part 2 ITER_D_2ES43V v2.0, 2012. https://user.iter.org/?uid = 2ES43V.